ORIGINAL PAPER

SERS-based immunoassay based on gold nanostars modified with 5,5′-dithiobis-2-nitrobenzoic acid for determination of glial fibrillary acidic protein

Peng Zhao[1] · Jingyi Sun[2] · Shijun Zhao[3] · Yanan Song[4] · Feng Gao[1] · Hongbin Wang[1] · Qingbin Ni[5] · Ying Wang[1] · Baoliang Sun[1]

Abstract

A surface-enhanced Raman scattering (SERS)–based immunoassay with gold nanostars (GNSs) is utilized for determination of the subarachnoid hemorrhage (SAH) biomarker glial fibrillary acidic protein (GFAP) at very low concentration levels, which allows for early diagnosis and guides clinical decision-making to treat SAH-induced complications. The Raman reporter 5,5′-dithiobis-2-nitrobenzoic acid (DTNB) modified on GNSs was selected as the SERS tags. The SERS immunoassay was assembled by SERS tag and GFAP probe-immobilized ITO substrate. Therefore, the level of GFAP can be detected by monitoring the characteristic Raman peak intensity of GFAP-conjugated GNSs at 1332 cm^{-1} with a very low detection limit. Under optimized conditions, the assay can work in the GFAP concentration range from 1 pg·mL^{-1} to 1 µg·mL^{-1}, with a detection limit as low as 0.54 fg·mL^{-1}. The performance of the SERS immunoassay proven by the detection of GFAP is equivalent to that of the conventional enzyme-linked immunosorbent assay (ELISA).

Introduction

Subarachnoid hemorrhage (SAH) is a devastating subtype of stroke that is life-threatening with high morbidity and mortality. Its pathological process involves the extravasation of blood into the subarachnoid space, which normally contains cerebrospinal fluid (CSF) [1]. Both clinical and experimental studies have shown that only a small number of SAH patients can recover almost all physical and mental functions, but most SAH events are accompanied by delayed cerebral ischemia (DCI), cerebral vasospasm (CVS), rebleeding, and other complications, which contribute to death and remain the major challenge of SAH [2, 3]. Timely initiation of treatment can prevent cerebral stroke, but sometimes the diagnosis of DCI and CVS can be elusive and treatment is often administered too late to reverse the damage [4].

In SAH patients, a range of brain-derived biomolecules are released into the CSF [5], the compositions of which reflect biochemical changes that occur in the brain [6]. Thus, the determination of brain-specific biomarkers in CSF can be helpful to assess damage to the brain, which allows for early diagnosis and guides clinical decision-making to treat SAH-induced complications [7, 8]. Glial fibrillary acidic protein (GFAP) is considered to be a brain-specific astrocyte intermediate filament protein in mature astrocytes that is very low in healthy individuals and shows an increase in both SAH-related CSF and serum [9]. The increase in GFAP

✉ Ying Wang
yingw9@163.com

Baoliang Sun
blsun88@163.com

1 Department of Neurology, Second Affiliated Hospital, Institute for Neurological Research & Key Laboratory of Cerebral Microcirculation, Shandong First Medical University & Shandong Academy of Medical Sciences, Taian 271000, Shandong, China

2 Shandong Provincial Hospital Affiliated To Shandong First Medical University& Shandong Academy of Medical Sciences, Jinan 250021, Shandong, China

3 Department of Neurology, Baotou Central Hospital, Baotou 014040, Neimenggu, China

4 Qingdao Medical College of Qingdao University, Qingdao 266021, Shandong, China

5 Postdoctoral Workstation, Taian Central Hospital, Taian 271000, Shandong, China
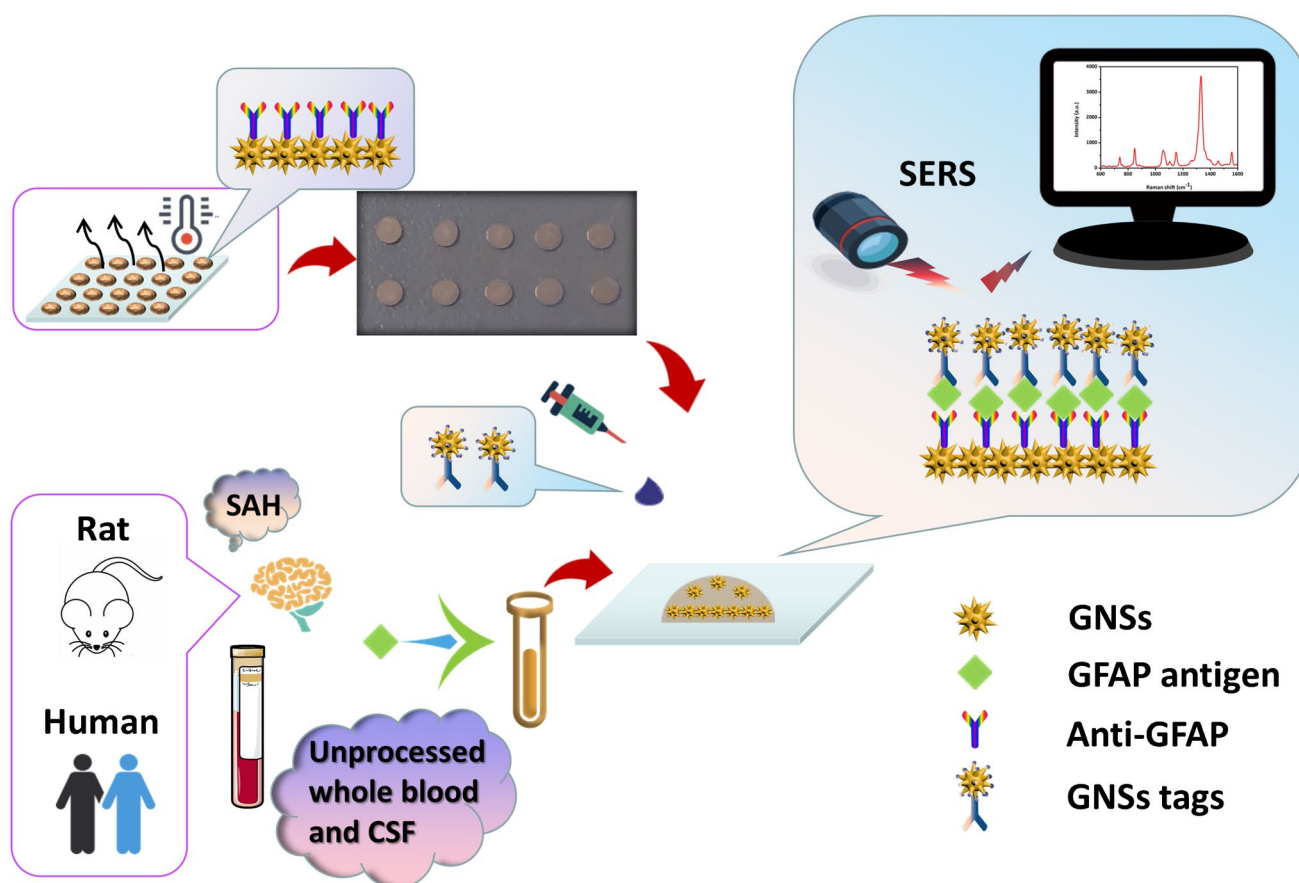
Scheme 1 Schematic illustration of GNSs SERS immunoassay for ultrasensitive dynamic change detection of GFAP (SAH, subarachnoid hemorrhage; SCF, cerebrospinal fluid; GNSs, gold nanostars; SERS, surface-enhanced Raman scattering; GFAP, glial fibrillary acidic protein)

levels caused by induced reactive astrogliosis reflects astrocyte damage and cell death [10], and these changes in astrocytes after SAH subsequently lead to the development of DCI and relevant long-term complications [11]. GFAP is a candidate biomarker for astrocytic damage that can monitor the early development of CVS and DCI after SAH, therefore influencing subsequent clinical management [12].

The current development of nanotechnology makes surface-enhanced Raman spectroscopy (SERS) a powerful platform with single-molecule-level sensitivity and quantitative detection capacities for chemical analysis and biomedical research [13, 14]. Compared with conventional immunoassays, SERS possesses many special advantages, such as no complex sample pretreatment, low reagent consumption, less water interference, better selectivity ability, good stability, convenience, and reproducibility [15–17]. Therefore, SERS is considered to be an ideal approach for the detection of water-containing samples [18] and is suitable for the detection of biomarkers in complex biological fluids, such as urine, blood plasma, and CSF [19, 20].

Herein, we report the development of SERS substrates based on plasmonic gold nanostars (GNSs) for GFAP detection

and the feasibility of their application in SAH diagnosis (Scheme 1). The low concentrations of GFAP in CSF and untreated whole blood collected from the SAH models and human samples were examined through SERS immunoassay. GFAP-specific SERS tagged GNSs@DTNB@Anti-GFAP were prepared by bioconjugation of GFAP antibodies and the Raman reporter DTNB onto the GNS surface. DTNB was used as a Raman reporter due to its high Raman activity [20, 21]. This SERS immunoassay shows good sensitivity, selectivity, and relatively low detection limits, so it offers a novel and suitable strategy for rapid early diagnosis of SAH-induced complications and has great application prospects in the clinic.

Experimental Section

Materials

Tetrachloroaurate (III) trihydrate (HAuCl$_4$·3H$_2$O), bovine serum albumin (BSA), and 5,5′-dithiobis-2-nitrobenzoic acid (DTNB) were acquired from Shanghai Chemical Reagent LTD, China (https://www.scrri.com). 1-[3-(Dimethylamino)

propyl]-3-carbodiimide hydrochloride (EDC), N-hydroxy-succinimide (NHS), and γ-mercaptopropyltriethoxy-silane (MPTES) were acquired from Sigma-Aldrich Chemicals (http://www.sigmaaldrich.com). Hydroquinone, dimercaptosuccinic acid (DMSA), ethanol, and phosphate buffered saline (PBS) (10 mM Na_2HPO_4, 1.8 mM KH_2PO_4, 2.7 mM KCl, 137 mM NaCl, pH = 7.4) were obtained from Shanghai Aladdin LTD, China (https://www.aladdin-e.com). GFAP standard grade antigens and anti-GFAP rat/human monoclonal antibodies were obtained from Sangon Biotech LTD, China (https://www.sangon.com). All other chemical reagents used were analytical grade or higher and can be used without further purification. Milli-Q-grade water (18.2 MΩ·cm) was used throughout all experiments.

Synthesis of GFAP labeling antibody modified SERS tags

Gold nanostars were synthesized according to a modified seed-mediated method, and SERS active GNS-tags were prepared using a previously reported method [22, 23]. The preparation of GNSs@DTNB@Anti-GFAP SERS nanotags is described in detail in the Supplementary Information.

Preparation of GFAP probe-immobilized SERS immunosubstrates

MPTES-functionalized indium tin oxide (ITO) conductive substrates were obtained according to the literature described previously [23, 24]. For the fabrication of the immunosubstrates, 5 μL of GNSs@Anti-GFAP was added dropwise on the MPTES-functionalized substrate to obtain GNS layers. Finally, the SERS substrates were further washed with ultrapure water three times and then dried at 30 °C for 30 min. Thus, GFAP probe-immobilized SERS immunosubstrates were obtained.

Animals

Approximately 12-week-old Sprague–Dawley (SD) rats (male, 280–330 g) were purchased from Shandong Experimental Animal Center (Jinan, China). Rats were housed with a 12-h light/dark cycle and free access to water and food. All experimental procedures and animal care were approved by Shandong First Medical University & Shandong Academy of Medical Sciences Ethics Committee and were in agreement with the guidelines of the National Institute of Health.

Rat SAH models

Rat SAH models were established by the single injection method and endovascular perforation method.

The single blood injection (SBI) SAH model was produced as previously described [25]. After the rat was anesthetized and the atlanto-occipital membrane was exposed, a 1-mL syringe with a 25-gauge needle was placed into the cistern magna. Then, 0.3 mL of autologous femoral artery blood was slowly injected into the cistern magna within 3 min by a syringe pump. Rats were allowed to recover 30 min after SAH.

The endovascular perforation (EP) SAH model was prepared according to a previously reported method [23]. Specifically, rats were initially anesthetized using chloral hydrate (350 mg/kg body weight). A blunted 4–0 monofilament nylon suture was injected into the left internal carotid artery, and the bifurcation of the anterior and middle cerebral arteries was punctured until breakthrough was felt [26]. The suture was subsequently withdrawn for induction of SAH. Sham-operated groups received the same process excluding puncture.

Clinical samples

The clinical study was approved by the ethical committee of Baotou Central Hospital. From January 2018 to December 2019, 50 patients with aneurysmal SAH between the ages of 43 and 65 years were enrolled in an observational study on CSF analysis.

The clinical status on admission was evaluated by the World Federation of Neurological Surgeons (WFNS) grade and Hunt-Hess grade. The severity of SAH was graded by Fisher scale based on radiological characteristics. The inclusion criteria were as follows: treatment of aneurysm < 24-h post rupture. CSF is collected by performing a lumbar puncture on patients 3 days after onset.

CVS was considered focal or diffuse transient stenosis of the cerebral artery caused by contraction of smooth muscle in the vascular wall, which was calculated by head computed tomography (CT) scan and transcranial Doppler (TCD). DCI was clinically defined according to the following criteria: a new focal neurological deficit continued for more than 1 h, and a new infarct was identified on a head CT scan.

Results and discussion

Preparation and characterization of the SERS immunosubstrates

The synthesized GNS were characterized using a scanning electron microscope by dripping onto aluminum foil. As shown in Fig. 1A, the nanoparticles had a star-shaped morphology with an average diameter of approximately 70 nm. Figure 1B shows that GNSs had a UV–visible absorption maximum at 650 nm. When comparing the SERS images
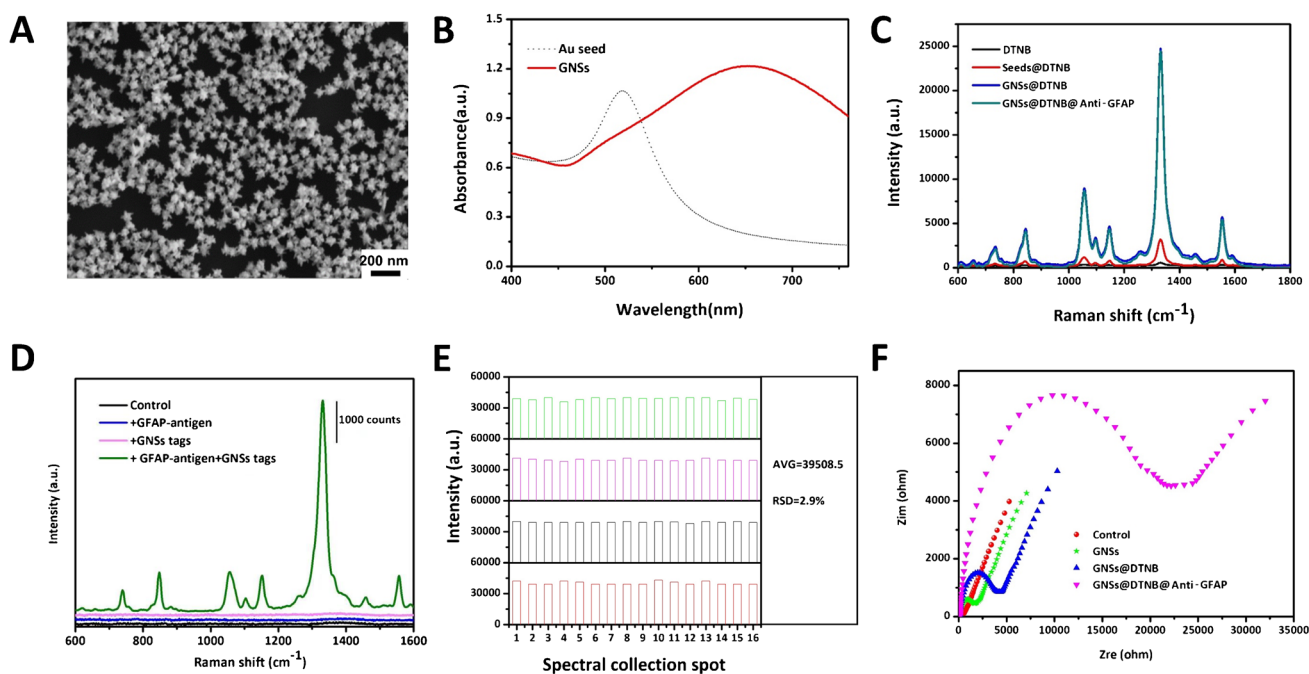
Fig. 1 **A** SEM image of gold nanostars. **B** UV–visible spectra of gold seeds and gold nanostars. **C** SERS spectra of gold seeds@DTNB, GNSs@DTNB, and GNSs@DTNB@Anti-GFAP. **D** SERS spectra of SERS tags detection process. **E** SERS intensity of tags at 1332 cm^{-1} was detected 50 times in four independent batches. **F** Electrochemical characterization of the SERS tag preparation process. EIS to record the immobilized steps of bare GCE (control), GNSs/GCE, GNSs@DTNB/GCE, GNSs@DTNB@Anti-GFAP/GCE

of gold seeds and GNSs modified by the Raman reporter DTNB, GNSs had a stronger enhanced Raman signal at 1332 cm^{-1}, and the labeling of GFAP antibody did not affect the Raman signal intensity of GNSs@DTNB (shown in Fig. 1C). In Fig. 1D, GNSs@Anti-GFAP were used as a substrate, and GNSs@DTNB@Anti-GFAP were used as SERS nanotags. There were no SERS signals when the analyte contained only GFAP antigen or SERS tags. When the analyte contained both GFAP antigen and SERS tags (which can form an immune "sandwich" structure), SERS signals can be detected. As presented in Fig. 1E, the SERS intensity of GNS tags at 1332 cm^{-1} was tested 50 times in four independent batches, with the results showing a deviation of 2.9% and verifying good reproducibility. The preparation process of SERS tags was characterized by electrochemical impedance spectroscopy [27]. Figure 1F shows the complex impedance plots of different layer modified electrodes (bare glassy carbon electrode (GCE) used as the control group) in the 5-mM [Fe(CN)6]$^{4-/3-}$ solution. This spectrum confirmed the successful combination of GNSs@DTNB@Anti-GFAP SERS tags.

Fabrication of GNS substrates is an important part of the immunosubstrates used for GFAP diagnosis in SAH patients. The preparation and characterization of the substrates are presented in the Supplementary Information. SERS 3D mapping was used for characterization and optimization of the substrates, and the results showed that the substrates had good stability and can be used in subsequent experiments (as shown in Fig. S1).

Optimization of the SERS immunoassay

Under optimal experimental conditions, the prepared SERS immunosubstrates can be used as an ideal tool for measuring different levels of GFAP biomarker incorporated in PBS buffer. Figure 2A reveals that the intensity of the SERS peak at 1332 cm^{-1} gradually rises with increasing of GFAP concentration (1 pg·mL^{-1}, 10 pg·mL^{-1}, 100 pg·mL^{-1}, 1 ng·mL^{-1}, 10 ng·mL^{-1}, 100 ng·mL^{-1}, 1 μg·mL^{-1}) in PBS. As illustrated in Fig. 2B, a good linear relationship was observed according to the corresponding calibration plot with a relative coefficient (R^2) of 0.99 and measurements ranging from 1 pg·mL^{-1} to 1 μg·mL^{-1}. The limit of detection (LOD) in PBS was lower than 1 fg·mL^{-1}, as shown in Fig. 2C. The calculations of LOD value was 0.54 fg·mL^{-1} using the formula LOD = 3σ/m (σ represents the standard deviation of the blank experiment, and m represents the slope of the linear measurement curve), which indicates that the SERS base immunosubstrates for GFAP antigen are sensitive and effective and can be used for GFAP detection. The stability of the SERS immunosubstrates was also evaluated by aging studies. The SERS immunosubstrates were placed
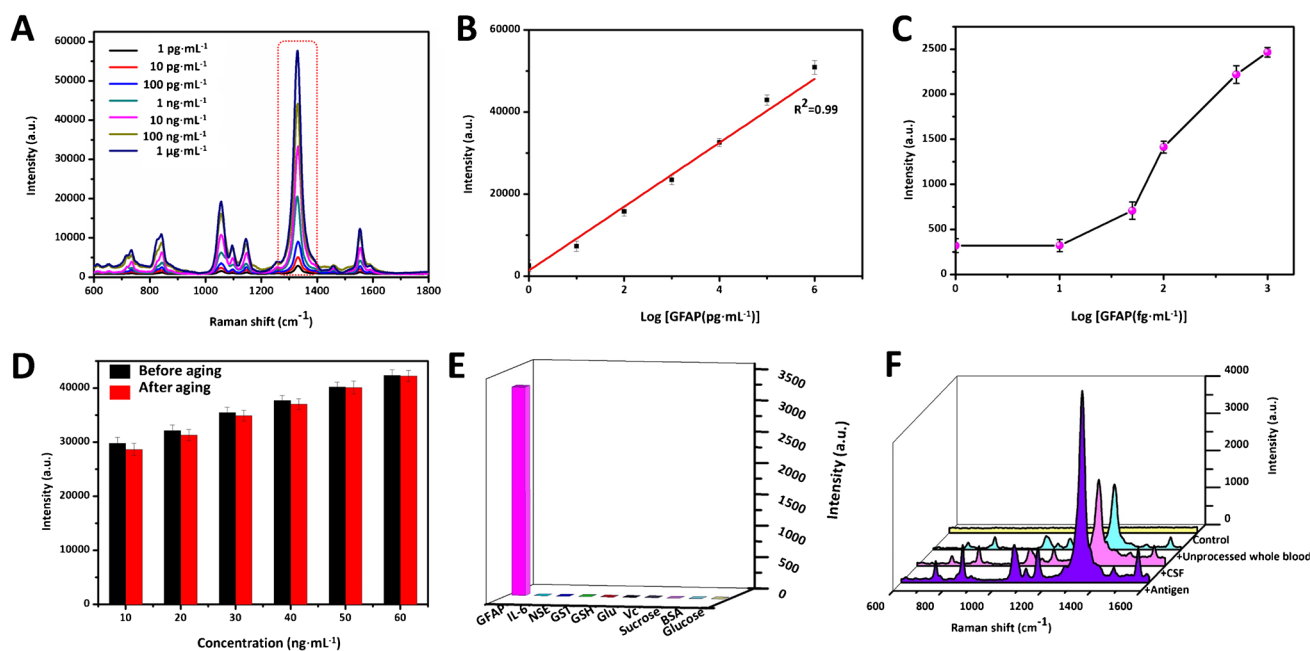
Fig. 2 A SERS spectra of SERS substrate with DTNB for detection of GFAP in PBS, ranging from 1 pg·mL^{-1}. to 1 μg·mL^{-1}. **B** Corresponding calibration plot of SERS peak intensity at 1332 cm^{-1} versus the logarithm value of GFAP concentration. **C** The LOD of GFAP in PBS. **D** SERS immunosubstrate performance evaluation: stability analysis before and after the accelerated aging test. **E** The selectivity of the immunosubstrates for different analytes (such as GFAP, IL-6, NSE, GS7, GSH, Glu, Vc, sucrose, BSA, and glucose). **F** SERS spectra of GFAP in PBS, CSF, and unprocessed whole blood

at 37 °C for 30 days, and GFAP was detected in PBS at six different concentrations (10 ng·mL^{-1}, 20 ng·mL^{-1}, 30 ng·mL^{-1}, 40 ng·mL^{-1}, 50 ng·mL^{-1}, 60 ng·mL^{-1}). There were no significant changes in SERS intensity at any GFAP concentration between freshly prepared immunosubstrates and the aging immunosubstrates, indicating that SERS-based immunosubstrates have good stability. The selectivity of the immunosubstrates was also analyzed, and the results are shown in Fig. 2E. Ten different analytes (GFAP, IL-6, NSE, GST, GSH, Glu, Vc, sucrose, BSA, glucose) at 10 ng·mL^{-1} were detected separately, and only the GFAP group had a strong SERE signal, indicating that these SERS immunosubstrates have good anti-interference ability. The feasibility of SERS immunosubstrates in clinical testing was also evaluated, and the results are shown in Fig. 2F. PBS was used as a negative control, 10 ng·mL^{-1} GFAP was used as a positive control, and then 10% GFAP solution was mixed with 90% CSF or unprocessed whole blood (from healthy SD rats). In Fig. 2F, both the CSF group and unprocessed whole blood group can detect SERS signals, indicating that SERS immunosubstrates can be used for body fluid testing. To study the potential clinical applications of SERS-based immunosubstrates, we contrasted their analytical performance with commercially available enzyme-linked immunosorbent assay (ELISA)

kits (data shown in Table S1).The results reveal that the method is comparable to ELISA.

Clinical applications

The feasibility of the SERS-based immunoassay was assessed by utilizing whole blood and CSF from a rat SAH model. First, rat SAH models were established by the single injection (SBI-SAH) method and endovascular perforation (EP-SAH) method. Three behavioral tests (activity, appetite, and deficits) (Table S3) and neurological scores (Table S5) were blindly evaluated at six different time points (ranging from 0 to 72 h) after SAH as previously reported [26–28]. After euthanasia, the basal brains were taken and photographed immediately, divided into six segments, and blindly evaluated from 0 to 3 (Table S4). In Fig. 3A, compared with the sham group, the neurological scores in all SAH groups (6 h to 72 h) were decreased, with a significant difference ($P < 0.05$). In Fig. 3B, there was a significant difference in SAH grade between the sham group and all SAH groups. In comparison to the sham group, the neurological scores were significantly decreased in all SAH groups. These results showed that rat SAH models were successfully established.

These SAH rats were used to evaluate the feasibility of SERS-based immunoassay in GFAP dynamic detection. The SERS-based immunoassay would provide information
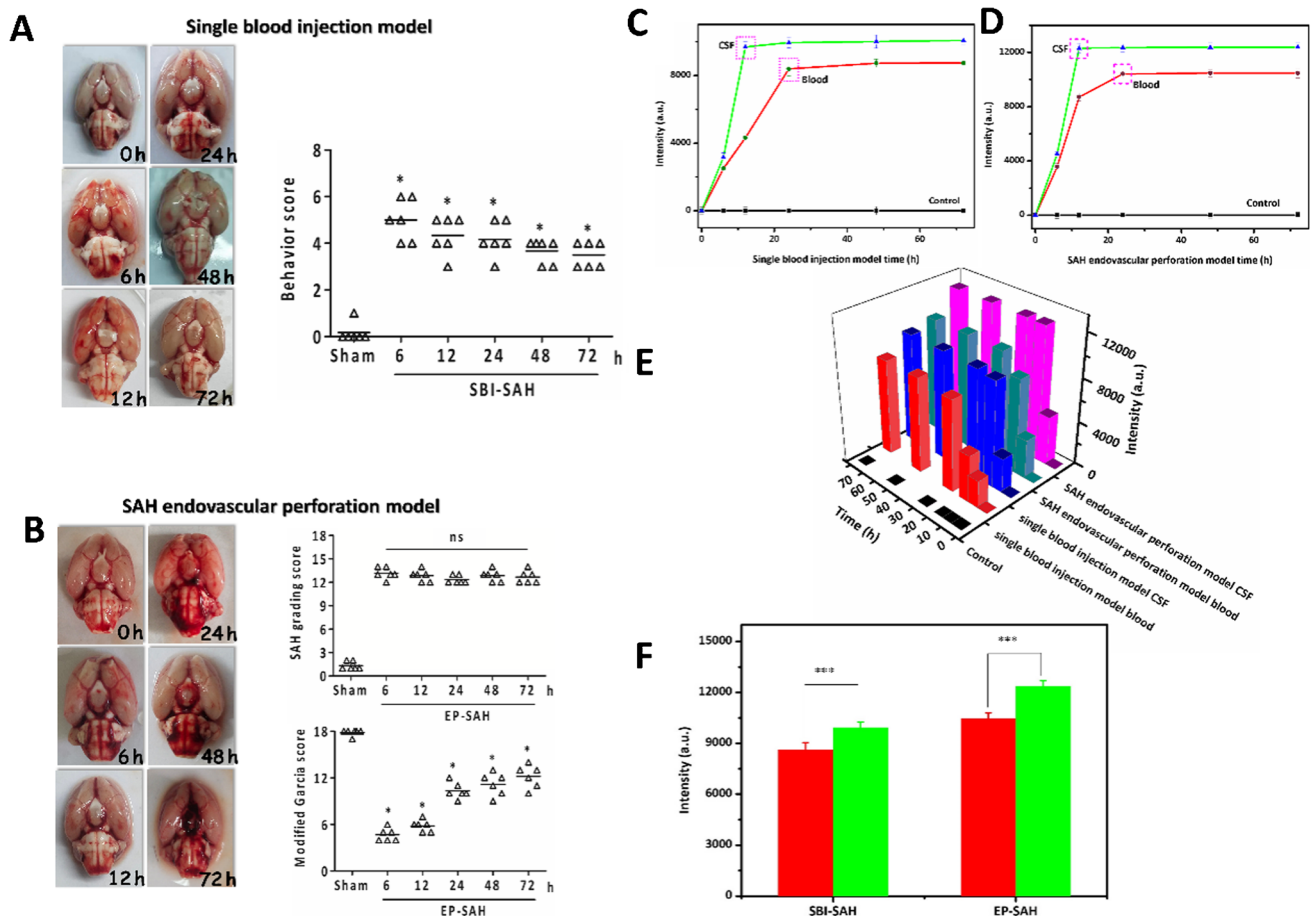
Fig. 3 Representative images of rat brains in the **A** SAH single blood injection model and **B** SAH endovascular perforation model. Neurological scores at 0 h, 6 h, 12 h, 24 h, 48 h, and 72 h. Raman intensities of analytes (untreated whole blood, CSF) at 1332 cm^{-1} from 0 to 72 h in both the **C** SBI-SAH model and **D** EP-SAH model. **E** Comparison of GFAP Raman intensities in all test groups. **F** Analysis of GFAP Raman intensity in the blood and CSF groups

concerning the possibility of SAH-related CVS or DCI. Whole blood and CSF were collected at 0 h, 6 h, 12 h, 24 h, 48 h, and 72 h after SAH. In Fig. 3C, GFAP can be detected by SERS-based immunoassay in both blood and CSF samples. In Fig. 3C, GFAP can be detected in both blood and CSF samples via SERS-based immunoassay. The GFAP SERS signal intensity gradually increased with time after SAH. In CSF samples, the signal intensity reached the peak after 6 h. In the blood sample, the signal intensity peaked after 12 h. The results in Fig. 3C show that the GFAP concentration in CSF increased faster than that in blood and reached the peak value earlier than that in blood. In EP-SAH rats (Fig. 3D), the results were consistent with SBI-SAH rats. Comparing all groups (Fig. 3E), it was found that the SERS intensity of GFAP in CSF was higher than that in blood. Statistical analysis of the SERS intensity of GFAP after the peak value (Fig. 3F) showed that the CSF groups were significantly higher than the blood groups ($P < 0.001$) in SBI-SAH and EP-SAH rats. These data indicate that the

concentration of GFAP in blood and CSF increases rapidly after SAH, and GFAP is more sensitive in CSF, making GFAP a candidate biomarker for SAH detection.

The feasibility of this SERS-based immunoassay was further assessed using human CSF, recorded information regarding CVS or DCI after SAH, and subsequently compared the above results with the outcome from traditional CT imaging. Figure 4 reveals the SERS signals of four CSF groups, the healthy patients (control group, $n = 15$), SAH patients without CVS or DCI (non-group, $n = 15$), CVS group ($n = 15$), and DCI group ($n = 15$), using the SERS-based immunosubstrates. After normalization of the spectrum, it was found that the GFAP intensity of CSF in all SAH groups increased sharply (Fig. 4G). After statistical analysis, the results showed that the Raman signal of GFAP in the complication SAH groups (CVS, DCI) was significantly higher than that in SAH (Non) group ($P < 0.01$). Comparing all SAH groups, the DCI group had the highest GFAP signal intensity. The results suggest that as SAH progresses or
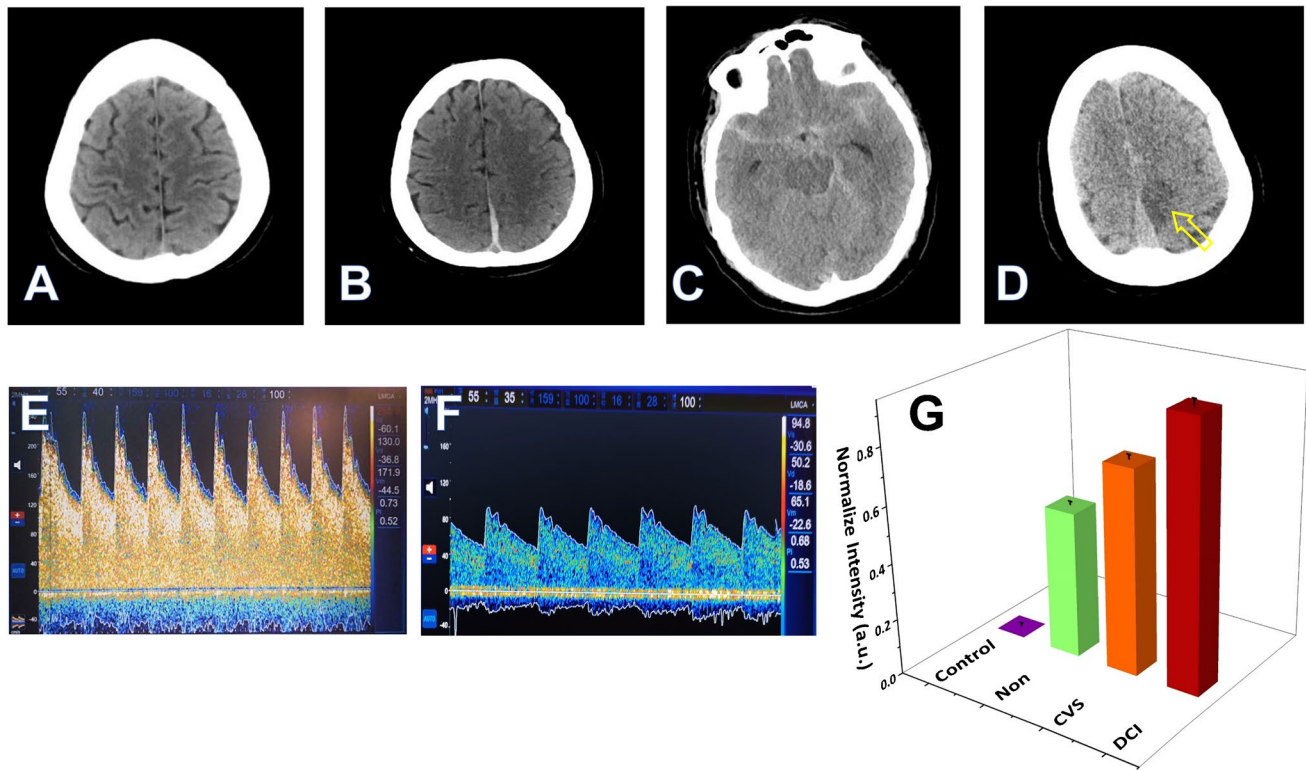
Fig. 4 A Head computed tomography (CT) scan of healthy patient. **B** One case of SAH patient, no delayed cerebral ischemia occurred during hospitalization, and CVS was not detected by transcranial Doppler (TCD). **C** One case of SAH patient 7 days after onset, TCD showed (Fig. 4E) that the middle cerebral artery flow velocity of left brain was 172 cm/s, which was significantly faster than the baseline mean blood flow velocity (Fig. 4F, Vm=65 cm/s); the Lindegaard Index was 4.7, suggesting cerebral vasospasm. **D** One case of SAH patient developed paralysis of the right lower extremity 4 days after onset. CT of the head showed a low-density shadow of the left parietal lobe (yellow arrow), suggesting acute cerebral infarction. **G** Comparison of GFAP Raman intensities of human CSF in all test groups (healthy patients, control group; SAH patients without DCI or CVS, non-group; DCI group; CVS group)

severity increases, the GFAP signal intensity also increases. CSF-derived GFAP levels are sensitive injury indicators that are elevated after SAH and reflect disease severity after SAH [6, 29], and the analysis results are consistent with those of previous reports. In addition, the results are also highly in agreement with CT imaging outcomes. Therefore, the SERS-based immunoassay is beneficial for the early detection of SAH-related latent complications using human CSF, and the method can be a potential detection method for the clinical diagnosis of SAH and SAH -induced complications.

Conclusions

Compared to conventional ELISA, this SERS immunoassay holds good sensitivity, selectivity, and stability and is extremely suitable for the early and rapid diagnosis of SAH-induced latent complications by applying human CSF samples. SERS-based immunoassay is a potential substitute for ELISA and greatly meets the demands of rapid detection to obtain more accurate results in a broad concentration range (from $pg\cdot mL^{-1}$ to $\mu g\cdot mL^{-1}$). The GFAP protein can be detected by this SERS immunoassay with very low detection limits by monitoring the intensity of the characteristic Raman peak of GFAP-conjugated GNPs at 1332 cm^{-1}. Under optimized conditions, the detection limit is as low as 0.54 $fg\cdot mL^{-1}$. The proven $fg\cdot mL^{-1}$ level detection would allow the determination of GFAP or biological compounds in complex biological fluids, which allows this SERS immunoassay to monitor the early development of CVS and DCI after SAH, therefore guiding subsequent clinical management and improving the prognosis of SAH patients. We anticipate that this SERS immunoassay can be further applied in the prediction of complications in various neurosurgical diseases. It is difficult for Raman spectrometers to perform bedside detection in neurosurgical disease, which hinders the SERS-based immunoassay applications for point-of-care tests. In future studies, we will focus on making the SERS immunoassay more portable and accurate.

Declarations

Conflict of interest The authors declare no competing interests.

References

1. Suarez JI, Tarr RW, Selman WR (2006) Aneurysmal subarachnoid hemorrhage. N Engl J Med 354:387. https://doi.org/10.1056/NEJMra052732
2. Kim W, Lee SH, Ahn YJ, Lee SH, Ryu J, Choi SK, Choi S (2018) A label-free cellulose SERS biosensor chip with improvement of nanoparticle-enhanced LSPR effects for early diagnosis of subarachnoid hemorrhage-induced complications. Biosens Bioelectron 111:59. https://doi.org/10.1016/j.bios.2018.04.003
3. Lawton MT, Vates GE (2017) Subarachnoid Hemorrhage. N Engl J Med 377:257. https://doi.org/10.1056/NEJMcp1605827
4. Al-Mufti F, Amuluru K, Smith B, Damodara N, El-Ghanem M, Singh IP, Dangayach N, Gandhi CD (2017) Emerging Markers of early brain injury and delayed cerebral ischemia in aneurysmal subarachnoid hemorrhage. World Neurosurg 107:148. https://doi.org/10.1016/j.wneu.2017.07.114
5. Lad SP, Hegen H, Gupta G, Deisenhammer F, Steinberg GK (2012) Proteomic biomarker discovery in cerebrospinal fluid for cerebral vasospasm following subarachnoid hemorrhage. J Stroke Cerebrovasc Dis 21:30. https://doi.org/10.1016/j.jstrokecerebrovasdis.2010.04.004
6. Rickard JJS, Di-Pietro V, Smith DJ, Davies DJ, Belli A, Oppenheimer PG (2020) Rapid optofluidic detection of biomarkers for traumatic brain injury via surface-enhanced Raman spectroscopy. Nat Biomed Eng 4:610. https://doi.org/10.1038/s41551-019-0510-4
7. Francoeur CL, Mayer SA (2016) Management of delayed cerebral ischemia after subarachnoid hemorrhage. Crit Care 20:277. https://doi.org/10.1186/s13054-016-1447-6
8. Stylli SS, Adamides AA, Koldej RM, Luwor RB, Ritchie DS, Ziogas J, Kaye AH (2017) miRNA expression profiling of cerebrospinal fluid in patients with aneurysmal subarachnoid hemorrhage. J Neurosurg 126:1131. https://doi.org/10.3171/2016.1.JNS151454
9. Ren C, Kobeissy F, Alawieh A, Li N, Li N, Zibara K, Zoltewicz S, Guingab-Cagmat J, Larner SF, Ding Y, Hayes RL, Ji X, Mondello S (2016) Assessment of serum UCH-L1 and GFAP in acute stroke patients. Sci Rep 6:24588. https://doi.org/10.1038/srep24588
10. Murakami K, Koide M, Dumont TM, Russell SR, Tranmer BI, Wellman GC (2011) Subarachnoid hemorrhage induces gliosis and increased expression of the pro-inflammatory cytokine high mobility group box 1 protein. Transl Stroke Res 2:72. https://doi.org/10.1007/s12975-010-0052-2
11. Anzabi M, Ardalan M, Iversen NK, Rafati AH, Hansen B, Ostergaard L (2018) Hippocampal atrophy following subarachnoid hemorrhage correlates with disruption of astrocyte morphology and capillary coverage by AQP4. Front Cell Neurosci 12:19. https://doi.org/10.3389/fncel.2018.00019
12. Jung CS, Lange B, Zimmermann M, Seifert V (2013) CSF and Serum biomarkers focusing on cerebral vasospasm and ischemia after subarachnoid hemorrhage. Stroke Res Treat 2013:560305. https://doi.org/10.1155/2013/560305
13. Laing S, Jamieson LE, Faulds K, Graham D (2017) Surface-enhanced Raman spectroscopy for in vivo biosensing. Nat Rev Chem 1:1. https://doi.org/10.1038/s41570-017-0060
14. Ding S, Yi J, Li J, Ren B, Wu D, Panneerselvam R, Tian Z (2016) Nanostructure-based plasmon-enhanced Raman spectroscopy for surface analysis of materials. Nat Rev Mater 1:1. https://doi.org/10.1038/natrevmats.2016.21
15. Sun F, Hung HC, Sinclair A, Zhang P, Bai T, Galvan DD, Jain P, Li B, Jiang S, Yu Q (2016) Hierarchical zwitterionic modification of a SERS substrate enables real-time drug monitoring in blood plasma. Nat Commun 7:13437. https://doi.org/10.1038/ncomms13437
16. Wang Y, Zhao P, Mao L, Hou Y, Li D (2018) Determination of brain injury biomarkers by surface-enhanced Raman scattering using hollow gold nanospheres. RSC Adv 8:3143. https://doi.org/10.1039/C7RA12410D
17. Li D, Yang M, Li H, Mao L, Wang Y, Sun B (2019) SERS based protocol using flow glass-hemostix for detection of neuron-specific enolase in blood plasma. New J Chem 43:5925. https://doi.org/10.1039/C8NJ02561D
18. Xiang S, Ge C, Li S, Chen L, Wang L, Xu Y (2020) In situ detection of endotoxin in bacteriostatic process by SERS chip integrated array microchambers within bioscaffold nanostructures and SERS tags. ACS Appl Mater Interfaces 374:1. https://doi.org/10.1021/acsami.0c04897
19. Kaminska A, Szymborski T, Jaroch T, Zmyslowski A, Szterk A (2018) Gold-capped silicon for ultrasensitive SERS-biosensing: Towards human biofluids analysis. Mater Sci Eng C 84:208. https://doi.org/10.1016/j.msec.2017.11.029
20. Zhao P, Li HX, Li DW, Hou YJ, Mao L, Yang M, Wang Y (2019) A SERS nano-tag-based magnetic-separation strategy for highly sensitive immunoassay in unprocessed whole blood. Talanta 198:527. https://doi.org/10.1016/j.talanta.2019.02.040
21. Rong Z, Xiao R, Xing S, Xiong G, Yu Z, Wang L, Jia X, Wang K, Cong Y, Wang S (2018) SERS-based lateral flow assay for quantitative detection of C-reactive protein as an early bio-indicator of a radiation-induced inflammatory response in nonhuman primates. Analyst 143:2115. https://doi.org/10.1039/c8an00160j
22. Shiohara A, Langer J, Polavarapu L, Liz-Marzan LM (2014) Solution processed polydimethylsiloxane/gold nanostar flexible substrates for plasmonic sensing. Nanoscale 6:9817. https://doi.org/10.1039/c4nr02648a
23. Wang Y, Sun J, Yang Q, Lu W, Li Y, Dong J, Qian W (2015) A SERS protocol as a potential tool to access 6-mercaptopurine release accelerated by glutathione-S-transferase. Analyst 140:7578. https://doi.org/10.1039/c5an01588j
24. Wang W, Han P, Xie R, Yang M, Zhang C, Mi Q, Sun B, Zhang Z (2019) TAT-mGluR1 attenuation of neuronal apoptosis through prevention of MGluR1α truncation after experimental subarachnoid hemorrhage. ACS Chem Neurosci 10:746. https://doi.org/10.1021/acschemneuro.8b00531
25. Wang Y, Yang Q, Sun J, Nie M, Dong J, Qian W (2016) Gold nanoflowers modified ITO glass as SERS substrate for carbon tetrachloride-induced acute liver injury in vitro detection. RSC Adv 6:115189. https://doi.org/10.1039/C6RA22706F
26. Wu Q, Qi L, Li H, Mao L, Yang M, Xie R, Yang X, Wang J, Zhang Z, Kong J, Sun B (2017) Roflumilast reduces cerebral inflammation in a rat model of experimental subarachnoid hemorrhage. Inflammation 40:1245. https://doi.org/10.1007/s10753-017-0567-8

27. Li R, Liu W, Yin J, Chen Y, Guo S, Fan H, Li X, Zhang X, He X, Duan C (2018) TSG-6 attenuates inflammation-induced brain injury via modulation of microglial polarization in SAH rats through the SOCS3/STAT3 pathway. J Neuroinflammation 15:231. https://doi.org/10.1186/s12974-018-1279-1

28. Lu W, Qian C, Bi L, Tao L, Ge J, Dong J, Qian W (2014) Bio-molecule-based formaldehyde resin microspheres loaded with Au nanoparticles: a novel immunoassay for detection of tumor markers in human serum. Biosens Bioelectron 53:346. https://doi.org/10.1016/j.bios.2013.10.007

29. Sugawara T, Ayer R, Jadhav V, Zhang JH (2008) A new grading system evaluating bleeding scale in filament perforation subarachnoid hemorrhage rat model. J Neurosci Methods 167:327. https://doi.org/10.1016/j.jneumeth.2007.08.004